Supplementary Information (SI) for Nanoscale Horizons.
This journal is © The Royal Society of Chemistry 2026

Supplementary Material:

Fluence-independent range of surface roughening within the Gaussian-shaped profile of a low-intensity ultrashort laser

Niklas Osterloh, Michael Vyshnepolsky, Tianluo Pan, and Karina Morgenstern*

Ruhr-Universität Bochum, Physical Chemistry I,

Universitätsstr. 150, D-44801 Bochum, Germany

(Dated: March 31, 2026)

Abstract

This supplementary information details the determination of the local coverage from the multitude of STM images and the local fluence responsible for the local coverage from the laser spot profile. It recapitulates the two-temperature model for determination of the transient electron and phonon temperature following the femtosecond-laser illumination with the parameters for copper and its references. Moreover, we supply the 400 original images that have been recorded in the series presented in Fig. 3 of the main manuscript.

DETERMINATION OF LOCAL COVERAGE

In the main text, we present fluence dependent and fluence independent local coverages. The coverage of a given image was determined on a randomly chosen region without secondary step edges of the image, ranging in area between 3000 nm^2 and 8500 nm^2. The region was cut out, and a plane was subtracted using the WSxM 5.0 software [1]. The coverage was determined using the flooding tool of WSxM 5.0. For multiple layers, the coverage of each layer was determined individually by setting different thresholds in the flooding tool. The overall coverage is displayed in Fig. 4 of the main manuscript.

Up to four regions with somewhat smaller areas between 300 nm^2 and 5000 nm^2, were analyzed to control that the random choice does not influence the results and to determine error bars. The same procedure was applied to both neighboring images in the image series. Subsequently, a weighted average and the corresponding standard deviation were calculated for the three images and displayed versus the local fluence in Fig. 4 of the main manuscript.

DETERMINATION OF THE LOCAL FLUENCE

In the main text, we discuss changes in surface texture in dependence of locally varying fluence across the Gaussian shaped laser spot. The shape of the laser spot on the surface was determined in-situ the STM by measuring the photoelectrons emitted from the Cu(511) surface while moving the STM tip over the laser spot on the surface in two perpendicular directions [2]. Note that at a laser energy of 3.1 eV, the photoelectron signal results from a two-electron process. The incoming laser spot profile is thus the square of the measured photoelectron signal.

The laser power was measured in a parallel setup, identical in number and type of optical elements to that of the STM setup, to account for energy losses by mirrors and windows. A slight deviation from the incoming beam direction by the movable in-situ mirrors was corrected by turning the thus determined Gaussian-shaped spot till images with similar coverage had a similar local fluence. Due to the wide distribution and the three branches observed in the measured images, the position of the spot center was clearly established. Finally, the local fluence is determined based on the average laser power distributed across the thus-determined laser spot profile.

TWO-TEMPERATURE MODEL

We estimate the highest electron T_{el} and phonon T_{ph} temperature reached in our experiment using the two-temperature model [3] in one dimension along the surface normal as detailed in [4]. Neglecting the lateral dimensions is justified because the typical electron diffusion lengths are considerably shorter than the laser spot diameter. Two differential equations couple the electron with the phonon temperature and describe their evolution in time:

$$C_{el}(T_{el})\frac{\partial}{\partial t}T_{el} = \frac{\partial}{\partial z}(\kappa_{el}\frac{\partial}{\partial z}T_{el}) - H(T_{el}, T_{ph}) + S(z,t) \tag{1}$$

$$C_{ph}(T_{ph})\frac{\partial}{\partial t}T_{ph} = \frac{\partial}{\partial z}(\kappa_{ph}\frac{\partial}{\partial z}T_{ph}) + H(T_{el}, T_{ph}) \tag{2}$$

with C_{el} and C_{ph} the heat capacities of the electron and phonon system, respectively, and κ_{el} and κ_{ph} their thermal conductivities. The first term describes the thermal diffusion along the z coordinate, the second term H couples the two subsystems, and S(z,t) reflects that the optical excitation is only adsorbed by the electron system.

The thermal conductivity of the electrons κ_{el} is given by [5]:

$$\kappa_{el} = \frac{1}{3}\nu_F^2\gamma\frac{T_{el}}{A(T_{el}^2) + B(T_{ph})} \tag{3}$$

with ν_F the Fermi velocity, γ the specific heat of the illuminated material, and A and B material specific constants.

In non-equilibrium, Eq. 3 reads:

$$\kappa_{el,neq} = \frac{1}{3}\nu_F^2\gamma\frac{T_{el}}{A(T_{el}^2 - T_{ph}^2) + \frac{1}{3}\nu_F^2\gamma\frac{T_{ph}}{\kappa_{el,eq}}} \tag{4}$$

with $\kappa_{el,eq}$, the heat conductivity in equilibrium, $T_{el} = T_{ph}$, from literature [9].

The electron-phonon coupling is calculated with time-dependent perturbation theory yielding [10]:

$$H(T_{el} - T_{ph}) = f(T_{el}) - f(T_{ph}) \tag{5}$$

with

$$f(T) = 4G(\frac{T}{\theta_D})^4 \int_0^{\frac{\theta_D}{T}} \frac{x^4}{e^x - 1} dx \tag{6}$$

with G the electron-phonon-coupling constant and θ_D the Debye temperature [6].

The optical excitation is given by:

$$S(z,t) = \frac{2}{\sqrt{\frac{\pi}{\log(2)}}} \frac{F}{t_{FWHM}} \alpha \exp(-4\log(2)(t/t_{FWHM})^2 - z\alpha) \tag{7}$$

with F the absorbed fluence, t_{FWHM} the temporal pulse half width, and α^{-1} the optical penetration depth. Subtracting the electronic heat capacity $C_{el} = \gamma T_{el}$ from the heat capacity of a crystal in equilibrium gives the phononic heat capacity C_{ph}.

Eqs. 1 and 2 are solved numerically using $\gamma_{Cu} = 96,8 J/(m^3 K^2)$ [6], $\nu_{F,Cu} = 1,57 \times 10^6 m/s$ [7], $A_{Cu} = 1,2 \times 10^7 (K^2 s)^{-1}$, $B_{Cu} = 0,05 \times 10^{-6} (mW^{-1})$ [8], $G_{Cu} = 1 \times 10^{17} W/(m^3 K))$ [11], and $\theta_{Cu} = 343K$, yielding the values stated in the main manuscript.

STM IMAGES FOR THE POSITION-DEPENDENT ALTERATION OF THE SURFACE TEXTURE

In Fig. 3 of the main text, we present individual images of the image series across the laser spot at increased size. Fig. S1 to S5 present the original images recorded along the first x branch (106 images), along the y branch (223 images), and the second x branch (71 images).

* karina.morgenstern@rub.de

[1] I. Horcas, R. Fernandez, J. M. Gomez-Rodriguez, J. Colchero, J. Gomez-Herrero, A. M. Baro, WSXM: A software for scanning probe microscopy and a tool for nanotechnology. Rev. Sci. Instrum. 78, 013705 (2007).

[2] C. Zaum, N. Osterloh, R. Darkins, D. Duffy, K. Morgenstern, Real-space observation of surface structuring induced by ultra-fast-laser illumination far below the melting threshold. Sci. Rep. 11, 13269 (2021).

[3] S. I. Anisimov, B. L. Kapeliovich, T. L. Perel'man, Sov. Phys. JETP 39, 375 (1974).

[4] C. Frischkorn, M. Wolf, Femtochemistry at Metal Surfaces: Nonadiabatic Reaction Dynamics. Chem. Rev., 106, 4207 (2006).

[5] C. Kittel, Introduction to solid state physics. Wiley, New York (1986).

[6] Z. Lin, L. V. Zhigilei, V. Celli, Electron-Phonon Coupling and Electron Heat Capacity of Metals under Conditions of Strong Electron-Phonon Nonequilibrium. Phys. Rev. B 77, 075133 (2008).

[7] N. W. Ashcroft, N. D. Mermin, Solid State Physics. Saunders College, Philadelphia, 1976.

[8] M. Kaveh, N. Wiser, Electron-Electron Scattering in Conducting Materials, Adv. Phys. 33, 257 (1984).

[9] Handbook of Chemistry and Physics, 56th edition, ed. R. Weast, CRC Press, Cleveland (1975).

[10] R. H. M. Groeneveld, R. Sprik, A. Lagendijk, Femtosecond Spectroscopy of Electron-Electron and Electron-Phonon Energy Relaxation in Ag and Au, PHys. Rev. B 51, 11433 (1995).

[11] J. Hohlfeld, S.-S. Wellershoff, J. Güdde, U. Conrad, V. Jähnke, E. Matthias, Electron and Lattice Dynamics Following Optical Excitation of Metals. Chem. Phys. 251, 237 (2000).

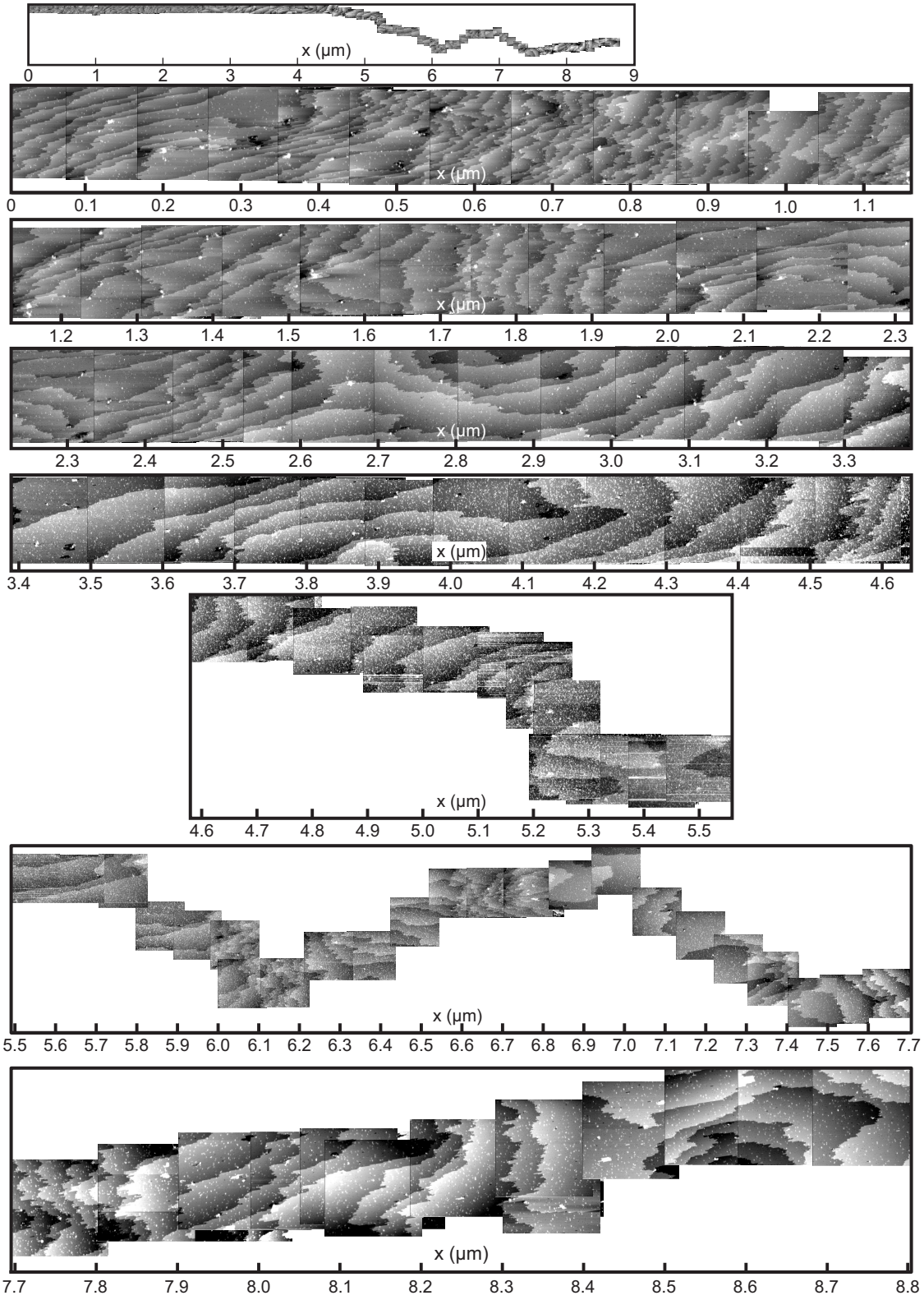

FIG. S1. STM images along the first x branch from x = 0 μm to 8.8 μm.

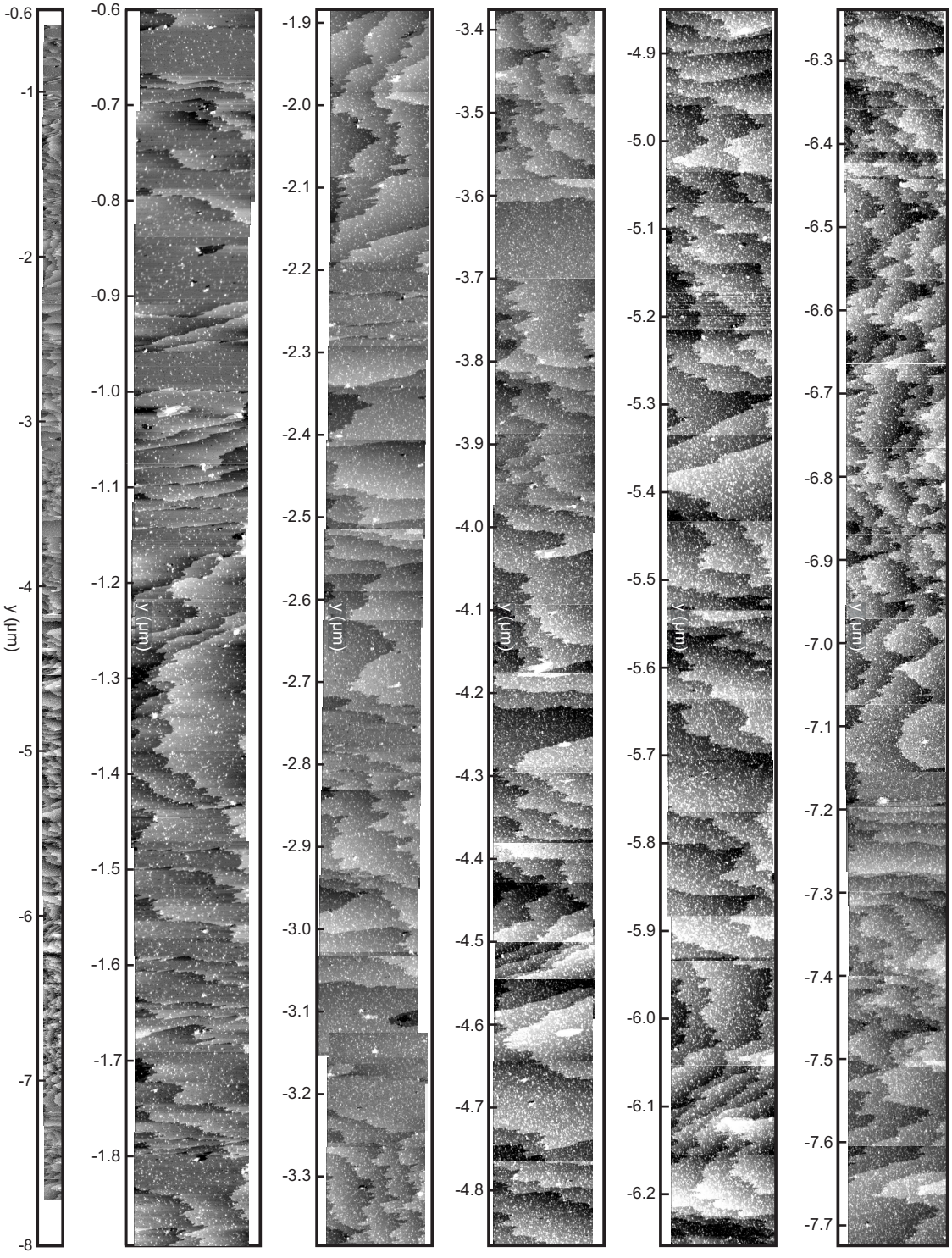

FIG. S2. STM images along the y branch from y = 0.6 μm to y = -7.7 μm.

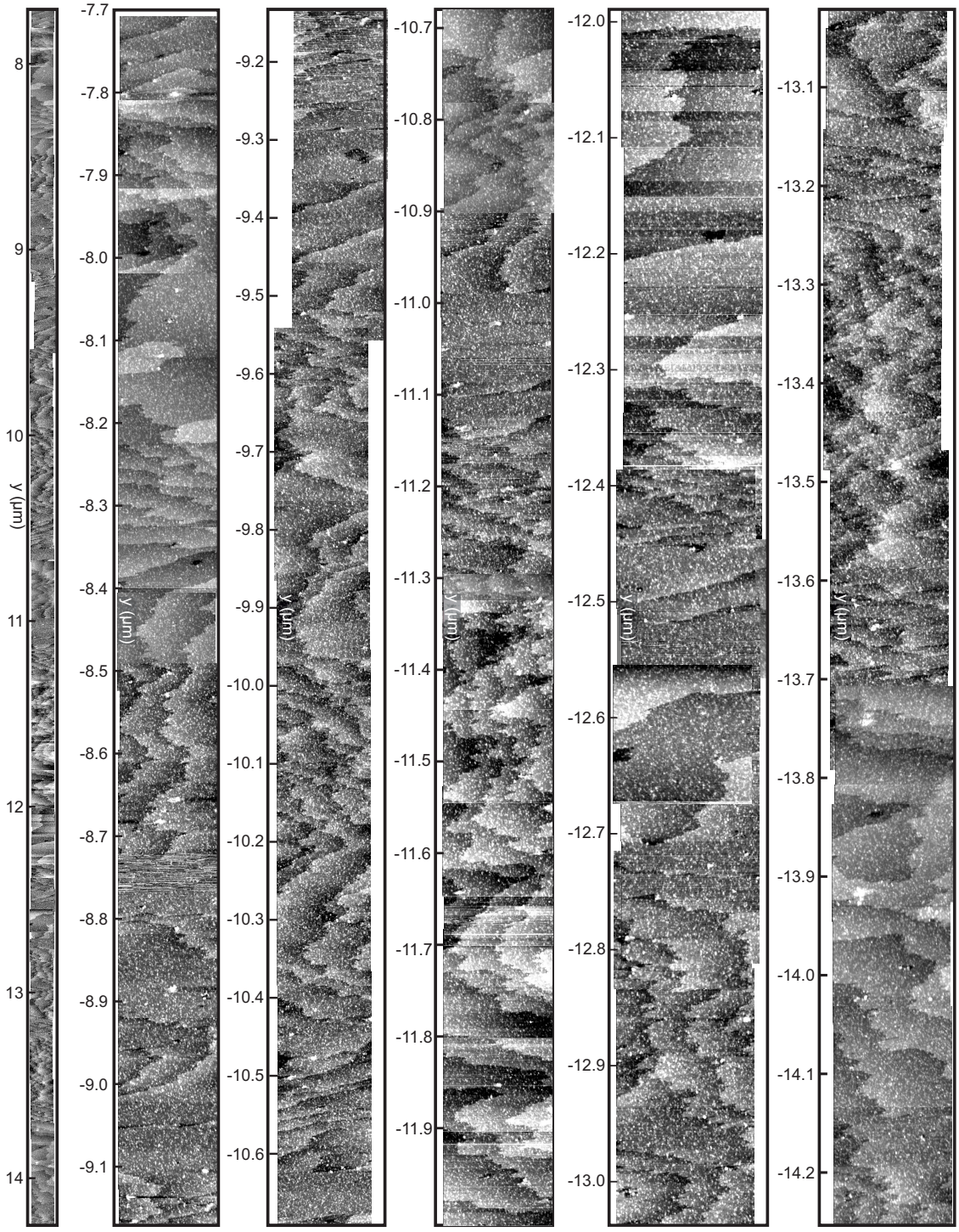

FIG. S3. STM images along the y branch from -7.7 μm to -14.2 μm.

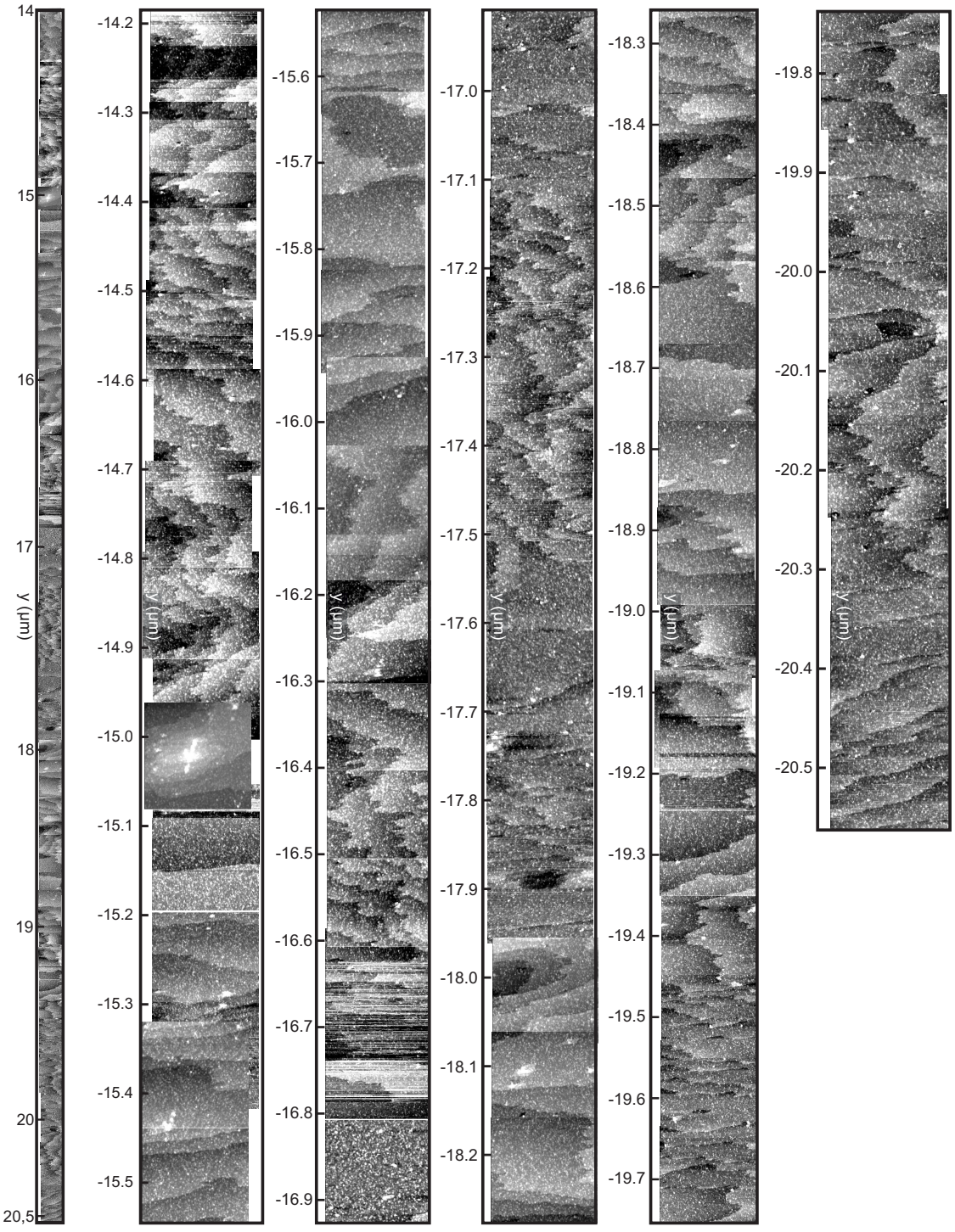

FIG. S4. STM images along the y branch from -14.2 μm to 20.5 μm.

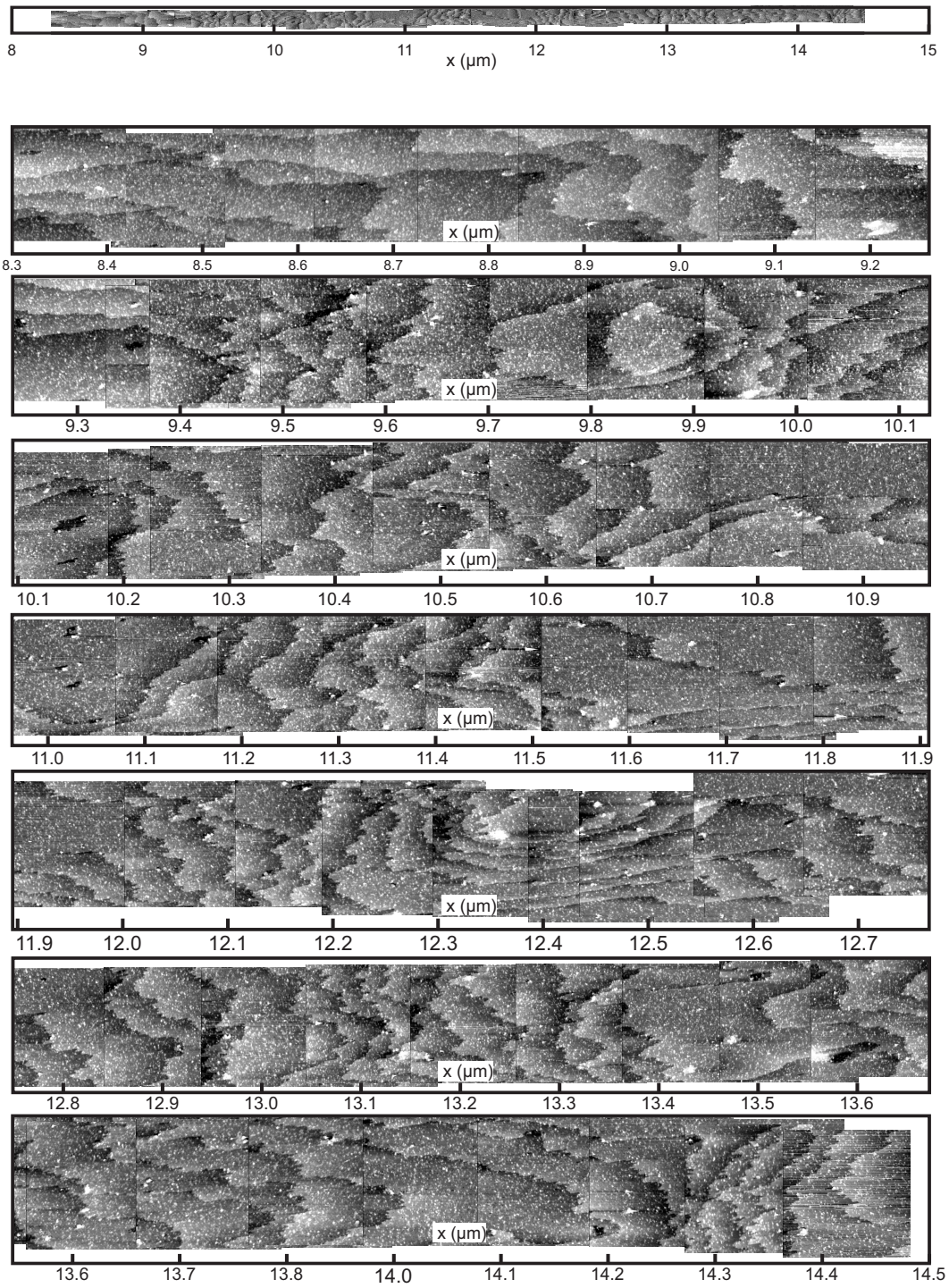

FIG. S5. STM images along the second x branch from x = 8.3 μm to 14.5 μm.